

Dynamic properties of high- T_c superconducting nano-junctions made with a focused helium ion beam

François Couëdo,¹ Paul Amari,¹ Cheryl Feuillet-Palma,¹ Christian Ulysse,² Yogesh Kumar Srivastava,^{3,4} Ranjan Singh,^{3,4} Nicolas Bergeal,¹ and Jérôme Lesueur,^{1*}

¹ *Laboratoire de Physique et d'Etude des Matériaux, CNRS,*

ESPCI Paris, PSL Research University, UPMC, 75005 Paris, France.

² *Centre de Nanosciences et de Nanotechnologie, CNRS, Université Paris Saclay, 91120 Palaiseau, France.*

³ *Division of Physics and Applied Physics, School of Physical and Mathematical Sciences, Nanyang Technological University, Singapore 637371, Singapore. and*

⁴ *Centre for Disruptive Photonic Technologies, The Photonics Institute,*

Nanyang Technological University, 50 Nanyang Avenue, Singapore 639798, Singapore.

(Dated: June 20, 2022)

We report on DC and RF properties of high- T_c Josephson Junctions fabricated by mean of a Helium ion beam focused at sub-nanometer scale, which locally modifies the superconductor. Starting from a 50 nm thick $\text{YBa}_2\text{Cu}_3\text{O}_7$ film, we made Josephson junctions with different irradiation doses from 200 to 600 ions/nm, and study their behavior as a function of temperature. Current-voltage characteristics are well fitted within the Resistively-Shunted-Junction (RSJ) model, suitable for Superconductor-Normal-Superconductor junctions. The characteristic frequency $f_c = (2e/h)I_c R_n$ reaches ~ 300 GHz at low temperature. We studied the AC Josephson effect in the frequency regime $f < f_c$ where clear Shapiro steps can be seen, whose width under 40 GHz irradiation was measured using the "detector response" method. We showed that the corresponding Josephson oscillation linewidth is only limited by the thermal noise in the RSJ model for temperature ranging from $T \sim 20$ K to 75 K. At lower temperature and for the highest irradiation dose, the shot noise contribution must also be taken into account when approaching the tunneling regime. We conclude that these Josephson nano-junctions present the lowest noise level possible, which makes them very promising for future applications in the microwave and terahertz regimes.

The astonishing recent evolution of Information and Communication Technologies (ICTs) is based on an accurate control of quantum properties of semiconductors at sub-micron scales. As some limitations appear, new paradigms emerge to further improve the performances of ICT devices, based on coherent quantum states and nano-scale engineering. Superconductivity is a very interesting platform which provides robust quantum states that can be entangled and controlled to realize quantum computation and simulation. It can also be used to make detectors of electromagnetic waves or photons operating at the quantum limit, *i.e.* with unsurpassed sensitivity and resolution, which can be used for classical or quantum communications [1–3]. Impressive results have been achieved in the recent years with the emergence of Quantum bits (Q-bits) based on Low critical Temperature (T_c) Superconductors (LTS) working well below liquid helium temperature[4]. Cryo-computers based on classical operations using the same materials are experimented as well[5]. The main building block of this superconducting electronics is the Josephson Junction (JJ), a weak link between two superconducting reservoirs. While the technology for LTS JJ of typically $1 \mu\text{m}$ in size required for complex systems is mature[5], other ways are explored to downsize the JJ using Carbon Nano-Tubes[6], Copper nanowires[7] or $\text{LaAlO}_3/\text{SrTiO}_3$ interfaces[8] for examples. The complexity and the cost of the needed cryogenic systems are clearly obstacles for large scale applications of such devices. High- T_c superconductors (HTS) operating at moderate cryogenic temperature (≤ 40 K) appear as an inter-

esting alternative solution, provided reliable JJ are available.

Different routes to make HTS JJ with suitable and reproducible characteristics are explored [9, 10]. One of them relies on the extreme sensitivity of HTS materials such as $\text{YBa}_2\text{Cu}_3\text{O}_7$ (YBCO) to disorder, which first reduces T_c and then makes it insulating. High energy ion irradiation (HEII) have been used to introduce disorder in YBCO thin films through e-beam resist masks with apertures at the nanometric scale (20 - 40 nm), to make JJ[11–13] and arrays[14–16] with interesting high frequencies properties, from microwaves to THz ones. Recently, Cybart *et al.* successfully used a Focused Helium Ion Beam (He FIB) to locally disorder YBCO thin films and make JJ[17]. In this technique, a 30 keV He^+ ion beam of nominal size 0.7 nm is scanned onto a thin film surface to induce disorder. Superconducting nano-structures and JJ have been fabricated with cuprate superconductors[18–22], MgB_2 [23] and pnictides[24]. While mainly DC properties of HTS JJ made by this technique have been reported to date, the present work aims at exploring their dynamic behavior, by studying the Josephson oscillation linewidth in the tens of GHz frequency range. This characterization, which gives access to the intrinsic noise of the JJ, is essential for high frequency applications of JJ such as mixers and detectors[13, 15, 16] and to study unconventional superconductivity[25].

Depending on the ion dose, HTS JJs made by the He FIB technique behave as Superconductor/Normal metal/Superconductor (SNS) JJs or Superconductor/Insulator/Superconductor (SIS) ones[17]. Müller *et al.*[22] evidenced scaling relations obeyed by the characteristic parameters I_c (critical current) and R_n (normal

* Corresponding author : jerome.lesueur@espci.fr

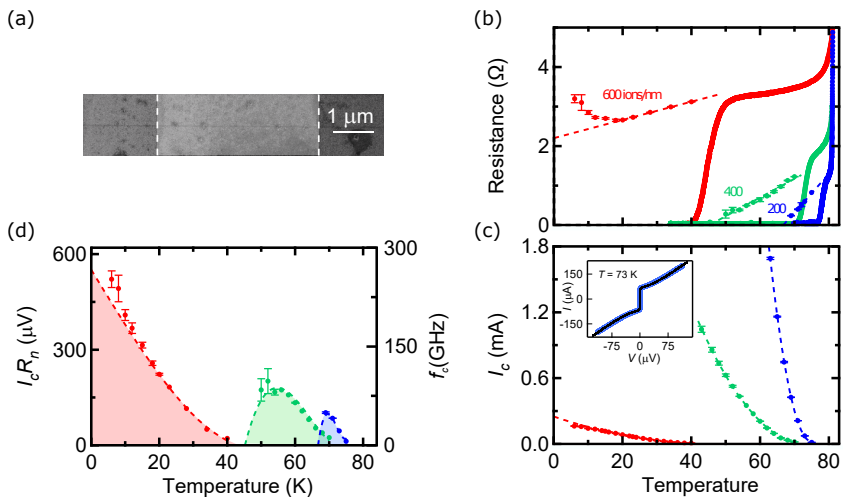


FIG. 1. (a) Image of a JJ using the imaging mode of the He-FIB microscope. The light grey area in between dashed lines is the superconducting channel defined by HEII. The horizontal line is the 600 ions/nm dose irradiated zone, which corresponds to the barrier of the JJ. (b) R vs T curves (solid lines) for JJ made using different irradiation doses: 200 ions/nm (blue), 400 ions/nm (green) and 600 ions/nm (red). Same color code for panels (c) and (d). Below T_J , R_n (symbols) is extracted from RSJ fits. Dashed lines show the linear decrease of $R(T)$ curves below T_J . (c) I_c vs T for different irradiation doses. Dashed lines are quadratic fits. *inset*: $I-V$ characteristics of a 200 ions/nm JJ. Blue line are data and black line is the RSJ fit. (d) $I_c R_n$ product vs T for different irradiation doses. Colored areas are calculated from the dashed lines in (b) and (c), and correspond to the Josephson regimes.

resistance), which are typical of highly disordered materials and known for a long time in HTS Grain-Boundary (GB) JJ[26] for example. The large density of localized electronic defect states at the origin of this behavior is a source of $1/f$ low-frequency noise[27, 28], which broadens the Josephson oscillation linewidth at much higher frequency[29]. To assess the potential performances of HTS Josephson devices made with He FIB, we directly measured the Josephson linewidth up to 40 GHz.

To fabricate HTS JJ, we begin with a commercial 50 nm-thick c-oriented YBCO thin film on a sapphire substrate[30] capped *in-situ* with 250 nm of gold for electrical contacts. After removing the Au layer by Ar^+ ion etching everywhere except at contact pads, we structure 4 μm wide and 20 μm long channels using the HEII technique[11]. An e-beam resist mask protects the film from a 70 keV oxygen ion irradiation at a dose of 1×10^{15} ions/cm² to keep it superconducting. The unprotected part becomes insulating. In a second step, samples are loaded into a Zeiss Orion NanoFab Helium/Neon ion microscope and the 30 keV He^+ beam (current ~ 1.15 pA) was scanned across the 4 μm -wide superconducting bridges to form JJs. A single line is used in these experiments, whose trace can be imaged directly in the microscope [22] (Figure 1 (a)). Imaging with the He^+ beam creates disorder, which adds to the one used to make the JJ. This is why we did not image the channels that we measured in the present study. On the same YBCO chip, we irradiated different channels with different doses ranging from 200 to 1000 ions/nm. The samples were then measured in a cryogen-free cryostat with a base temperature of 2K, equipped with filtered DC lines. The RF illumination is performed via a broadband spiral antenna placed 1 cm above the chip, and connected to a generator in a Continuous Wave (CW) mode at frequency f . To measure the "detector response" described below, the RF signal is electrically modulated at low frequency ($f_{\text{mod}} = 199$ Hz). The output signal is measured via a lock-in amplifier synchronized on this frequency.

Figure 1 (b) shows the resistance R as a function of temperature T for samples irradiated with a dose of 200, 400 and

600 ions/nm. Below the T_c of the reservoirs ($T_c = 84$ K), a resistance plateau develops till a transition to a zero-resistance state takes place, corresponding to the Josephson coupling through the irradiated part of the channel. Let T_J be this coupling temperature, which decreases as the dose is increased as already reported[17][22]. The resistance above T_J increases with disorder as expected, from $\lesssim 1$ Ω (200 ions/nm) to ~ 3 Ω (600 ions/nm). For irradiation dose higher than 1000 ions/nm, an insulating behavior is observed down to the lowest temperature. For the samples studied here (doses between 200 and 600 ions/nm), we measured the current-voltage ($I-V$) characteristics below T_J . The inset of Figure 1 (c) shows the $I-V$ curve of the 200 ions/nm sample recorded at $T = 73$ K, which can be accurately fitted with the Resistively-Shunted-Junction (RSJ) model including thermal noise (black line), as already reported[17, 22]. The RSJ fits are still valid when the dose and the temperature are varied, as proved by extended fits shown in Figure 2. From these fits, we extracted the temperature-dependent normal-state resistance $R_n(T)$ and the critical current $I_c(T)$ presented in Figure 1 (b) and (c), respectively. The former roughly follows the $R(T)$ curve measured above T_J , decreases linearly with temperature (dashed lines) and goes to zero at the superconducting temperature of the irradiated part where the Josephson regime ends. The latter has a quadratic temperature dependence (dashed lines) as expected for SNS JJ[11, 31]. Its absolute value can exceed 1 mA (200 and 400 ions/nm doses), which corresponds to critical current densities larger than 500 kA/cm²[22]. We show in Figure 1 (d) the $I_c R_n$ product as a function of temperature for the different irradiation doses. At low doses, it shows a maximum, characteristic of SS'S junctions (where S' is a superconductor with a T_c lower than the one of S) as observed with HEII HTS JJ[13]. However, for the highest dose (600 ions/nm), it raises monotonically as the temperature is lowered. Its maximum value ($I_c R_n \sim 600$ μV at 4 K) lies in between the values reported by Cybart *et al.*[17] and Müller *et al.*[22]. The corresponding characteristic frequency $f_c = I_c R_n / \Phi_0 \sim 300$ GHz ($\Phi_0 = h/2e$ the flux quantum) is higher than the one obtained by the HEII technique, which is promising for operations up to the THz

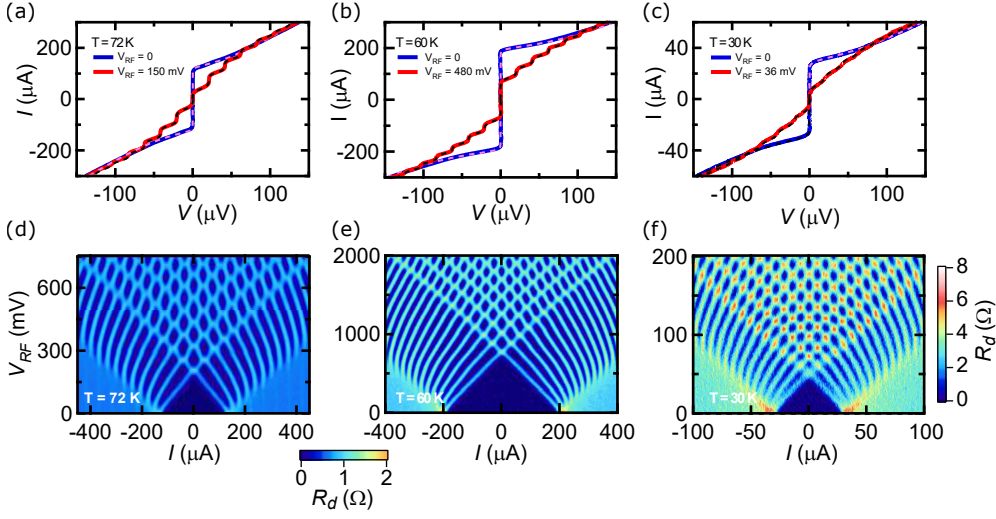


FIG. 2. $I-V$ characteristics of (a) a 200 ions/nm JJ, (b) a 400 ions/nm JJ and (c) a 600 ions/nm JJ, with (red) and without (blue) 10 GHz irradiation. Solid lines are data and dashed lines RSJ fits. Color-plot of R_d as a function of I and V_{RF} at $f = 10$ GHz for (d) a 200 ions/nm JJ and (e) a 400 ions/nm JJ (Color-scale at the bottom). (f) Same plot for a 600 ions/nm JJ (Color scale on the right).

frequency range[13].

We now focus on properties of these JJ at frequencies f much lower than f_c , and more specifically on the Shapiro steps which appear on $I-V$ characteristics at voltages $V_n = n \cdot f \cdot \Phi_0$ (n is an integer). Figure 2 (a) shows the $I-V$ curves of the 200 ions/nm JJ measured at $T=72$ K without (blue) and with (red) RF irradiation at $f = 10$ GHz, where we observe clear Shapiro steps. Both curves are well fitted with the RSJ model (dashed lines) with the following parameters : $R_n = 0.5 \Omega$, $I_c = 133 \mu A$ and for the RF curve : $I_{RF} = 133 \mu A$ (the RF current). For this temperature close to $T_J = 75$ K, R_n does not depend on the bias current I , contrary to the HEII HTS JJ[14, 32]. Swiping both the RF voltage V_{RF} and the bias current I , we recorded the $I-V$ curves from which we computed numerically the differential resistance $R_d = \frac{dV}{dI}$. The result is presented in color-scale in Figure 2 (d). The observation of well-defined and high-index (up to $n=12$) Shapiro steps attests the quality of this SNS JJ. Similar measurements were performed on the other JJs. The results are shown in Figure 2 (b) and (c) for the 400 ions/nm JJ and the 600 ions/nm, respectively. In each case, the measurement temperature ($T=60$ K and $T=30$ K) are close to their respective T_J . In this regime, all the curves are very well fitted with the RSJ model with the following parameters : $R_n = 0.68 \Omega$, $I_c = 205 \mu A$ and $I_{RF} = 143.5 \mu A$ for the 400 ions/nm JJ, and $R_n = 2.9 \Omega$, $I_c = 32.5 \mu A$ and $I_{RF} = 26.2 \mu A$ for the 600 ions/nm one. It is important to note that the RSJ fits were performed while taking a noise temperature equals to the bath temperature. Figures 2 (e) and (f) show color-plot for the corresponding samples. In both cases, pronounced oscillations with RF voltage corresponding to high order Shapiro steps are observed.

Shapiro steps unveil the internal Josephson oscillation that is produced when a JJ is biased beyond its critical current. The width of the steps is the linewidth of the Josephson oscillation[29]. Within the RSJ model, Likharev and Semenov[29, 33] calculated the voltage power spectral density $S_V(f)$ and the resulting Josephson oscillation linewidth Δf as follows : $\Delta f = \frac{4\pi}{\Phi_0^2} \cdot k_B T \cdot \frac{R_d^2}{R_n} \cdot \left(1 + \frac{I_c^2}{2I^2}\right)$ This thermal

Δf is the minimum Josephson linewidth which can be measured, as any other noise source will increase this intrinsic linewidth. Divin *et al.* showed that Δf can be measured experimentally from the Shapiro steps by mean of the "detector response" method[34–36]. The JJ is DC biased while the RF illumination is modulated at low frequency (f_{mod})[37]. The "detector response" signal V_{det} is measured with a lock-in amplifier synchronized at f_{mod} , and plotted as a function of the DC voltage V converted into a frequency f through the Josephson relation $f = V/\Phi_0$. Centered on the Josephson frequency, *i.e.* on the Shapiro step, an odd-symmetric structure appears, whose width (distance between the extrema) corresponds to Δf . To be more precise, Divin *et al.*[34] showed that the inverse Hilbert transform of the quantity $g(V) = (8/\pi) \cdot (V_{det}/R_d) \cdot I \cdot V$ is directly $S_V(f)$, a Lorentzian of width Δf centered at the Josephson frequency f . This procedure, successfully used in LTS[35] and HTS[36] materials, allows to extract the Josephson linewidth accurately.

We measured the Josephson oscillation linewidth of the different JJ irradiated at $f = 40$ GHz using the "detector response" method. Figure 3 (a) (bottom panel) shows V_{det} (left axis) as a function of the frequency ($f = V/\Phi_0$) for the 200 ions/nm JJ. Around 40 GHz, the characteristic double-peak structure predicted by Divin[34] is observed, from which we extracted the Josephson linewidth ($\Delta f = 4.87$ GHz). It is worth noticing that this method is highly sensitive, since the Shapiro steps cannot be seen in the $I-V$ curve simultaneously recorded (top panel). We then computed S_V through the above explained procedure, and plotted it on the same graph (Figure 3 (a) (bottom panel, right axis)). Two peaks are observed, corresponding to the first and second Shapiro steps, that can be fitted with Lorentzian to extract the corresponding Josephson oscillation linewidths. For the first step (index $n = 1$), the value is exactly the same as the one calculated above. Depending on the experimental conditions, we could accurately measure the Josephson linewidth of the first two Shapiro steps, or only of one of them.

We measured V_{det} as a function of V at different temperatures, as for example reported in Figure 3 (b) for the 400

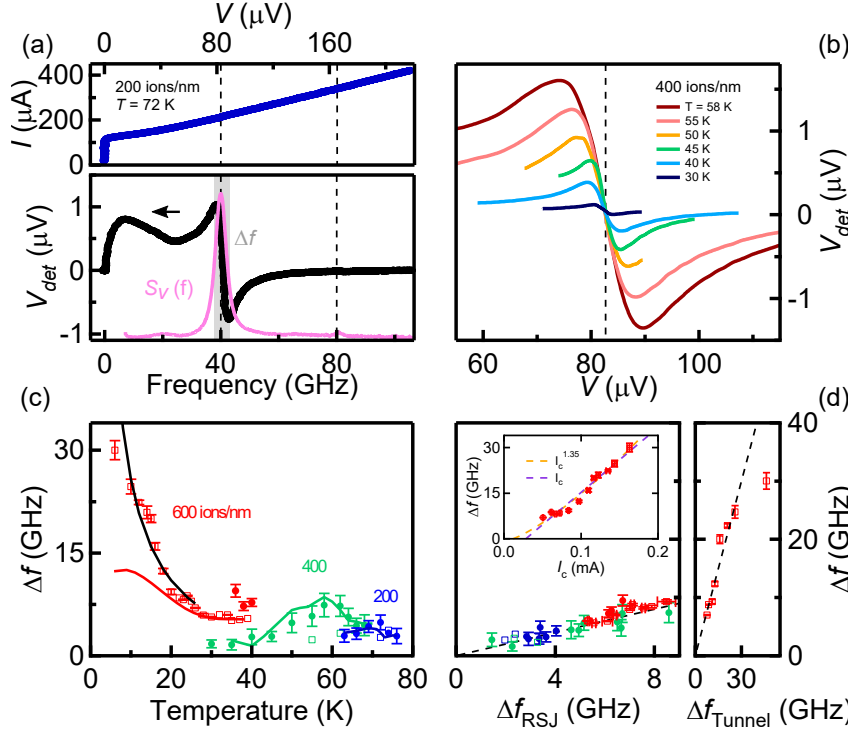


FIG. 3. (a) $I-V$ characteristics of the 200 ions/nm JJ under $f = 40$ GHz irradiation. V_{det} vs $f = V/\Phi_0$. The distance Δf between the extrema corresponds to the Josephson oscillation linewidth. S_V extracted from the inverse Hilbert transform of the normalized response $g(V)$ (pink), whose width is Δf (grey). (b) V_{det} vs V for a 400 ions/nm JJ measured at different temperatures under $f = 40$ GHz irradiation. (c) Δf vs T for different irradiation doses. Solid symbols correspond to the first Shapiro step, open symbols to the second one. Solid lines (blue, green, red) are calculated from the RSJ model for $n = 1$ (200 and 400 ions/nm) and $n = 2$ (600 ions/nm), the black one from the tunneling one. (d) Δf vs Δf_{RSJ} (left panel) and vs Δf_{Tunnel} (right panel), 600 ions/nm JJ ($n = 2$) for $T \leq 26K$. The slope of the dashed lines is one. *inset*: Δf vs I_c for the 600 ions/nm JJ ($n = 2$) for $T \leq 26K$. Dashed lines are best fits with a power-law exponent 1 (purple) and 1.35 (orange).

ions/nm JJ. The odd-symmetric structure at $V = 82.7\mu\text{V}$ (corresponding to 40 GHz, dashed line) widens with increasing temperature as expected for thermal noise. We extracted Δf as a function of temperature for the different samples. The result is shown in Figure 3 (c). Open (respectively solid) symbols correspond to measurements on the first (respectively second) Shapiro step. On the same graph, we added the linewidth Δf_{RSJ} calculated for the thermal noise in the RSJ model using the above equation[29, 33], *with no adjustable parameter*. The agreement is excellent for the 200 and 400 ions/nm JJ at all temperatures. For the 600 ions/nm, data are well reproduced at high temperature, but strongly depart from the calculation below $T = 20$ K. In Figure 3 (d), we made a parametric plot of the same data: the experimental Δf as a function of the calculated Δf_{RSJ} in the RSJ model with thermal noise (left panel). All data align along the dashed line of slope 1, which means that noise in He FIB JJ is purely thermal, except for 600 ions/nm JJ at low temperature.

This indicates that an extra source of noise takes place below $T = 20$ K in this JJ. We notice that this temperature corresponds to an up-turn in the $R(T)$ curve (Figure 1 (b)), which points towards a SIS-like JJ, as already reported by Cybart *et al.* for high irradiation doses[17]. In that case, the tunneling approach proposed by Dahm *et al.*[38] is more appropriate than the RSJ one to calculate the Josephson oscillation linewidth, which includes the non-linear superposition of thermal and shot noises in these JJ at intermediate damping[29, 38]. In that case: $\Delta f = \frac{4\pi}{\Phi_0^2} \cdot k_B T \cdot \frac{R_d^2}{nf\Phi_0} \cdot I$. We calculated Δf for the 600 ions/nm JJ with this expression, and obtained a very good agreement with the data as shown in Figure 3 (c)(black line), once again *with no adjustable parameter*.

The excess noise comes therefore from the shot noise contribution when approaching the tunneling limit. The parametric plot of the experimental Δf as a function of the calculated Δf_{Tunnel} including the shot noise (Figure 3 (d) right panel) clearly shows that there is no additional noise source in our JJ.

This seems quite surprising, given the recent result from Müller *et al.* pointing towards highly disordered JJ[22], which are usually associated with strong $1/f$ Flicker noise[27]. They measured the low-frequency noise of SQUIDS made with low-irradiation dose JJ (230 ions/nm). A clear $1/f$ noise component is observed up to ~ 100 kHz. These measurements have been performed on JJ fabricated on the so-called "LSAT" substrate, which have much lower I_c and $I_c R_n$ products than the others for the same dose. The role of the substrate on the JJ characteristics is not understood yet, but it is clear that the microstructure of the film matters for final JJ performances, and more specifically for noise properties related to defects. This has been evidenced long ago on YBCO Grain-Boundary JJ by annealing experiments[39, 40]. Our samples grown on sapphire may have therefore less fluctuating centers at the origin of Flicker noise than others. Past studies showed that this noise in HTS JJ is often induced by enhanced critical current fluctuations in inhomogeneous barriers[41–43], and that the maximum $1/f$ noise power in the vicinity of I_c scales with it ($S_{Vmax} \propto I_c^{2.7}$)[44][43]. This noise translates into a broader Josephson linewidth at high frequency, especially when $f < f_c$, *i.e.* for DC bias current close to I_c [36]. It has been evaluated by Hao *et al.*[45] as: $\Delta f = n \cdot \frac{2\pi}{\Phi_0} \cdot \sqrt{2S_V(f_0)} \cdot \ln\left(\frac{f_c}{f_0}\right)$ where f_0 is a low frequency cut-off of the $1/f$ noise (typically $f_0 \sim 1$ Hz). Through the above mentioned scaling relation,

Δf should thus increase as $I_c^{1.35}$ or so. The data on our 600 ions/nm sample below $T = 20$ K are compatible with this relation (inset Figure 3 (d)), but we cannot make a quantitative fit since we do not know the value of $S_V(f_0)$. Moreover, the same data can be fitted with the shot noise model as well (inset Figure 3 (d)), since the latter states that $\Delta f \sim I_c$ close to I_c (derived from the above equation). This model fits quantitatively the evolution of Δf with temperature with no adjustable parameter, and qualitatively the one with the critical current. We therefore conclude that the shot noise contribution fully explains the low temperature data of the most irradiated JJ, and that there is no evidence of strong Flicker noise in the present study.

We fabricated HTS JJ by the He FIB technique, and studied their DC and RF properties in the 10 to 40 GHz range. Their $I_c R_n$ product reaches 300 GHz at low temperature, which is higher than for HEII JJ. We showed that Shapiro steps in the $I - V$ characteristics that appear under RF irradiation are well described by the RSJ model for SNS junctions with thermal noise. Using the "detector response" method, we determined the Josephson oscillation linewidth, and showed that it corresponds to the sole Johnson-Nyquist thermal noise in the RSJ

model for the low-dose irradiated JJ. Below $T = 20$ K, the high-dose irradiated sample has a SIS character. We demonstrated that the associated enhanced noise is due to shot noise when approaching the tunneling regime. We did not evidenced any Flicker noise component, which means that the barrier is rather homogeneous in these JJ. This study paves the way for using He FIB JJ in high frequency applications[46].

I. ACKNOWLEDGEMENTS

The authors thank Yann Legall (ICUBE laboratory, Strasbourg) for ion irradiations. This work has been supported by the QUANTUMET ANR PRCI program (ANR-16-CE24-0028-01), the T-SUN ANR ASTRID program (ANR-13-ASTR-0025-01), the Emergence Program from Ville de Paris and by the Région Ile-de-France in the framework of the DIM Nano-K and Sesame programs.

BIBLIOGRAPHY

-
- [1] I. Holzman and Y. Ivry, *Advanced Quantum Technologies* **2**, 1800058 (2019).
 - [2] F. Sizov, *Semiconductor Science and Technology* **33**, 123001 (2018).
 - [3] O. Mukhanov, G. Prokopenko, and R. Romanofsky, *IEEE Microwave Magazine* **15**, 57 (2014).
 - [4] G. Wendin, *Reports on Progress in Physics* **80**, 106001 (2017).
 - [5] S. K. Tolpygo, *Low Temperature Physics* **42**, 361 (2016).
 - [6] J. P. Cleuziou, W. Wernsdorfer, V. Bouchiat, T. Ondarçuhu, and M. Monthieux, *Nature Nanotechnology* **1**, 53 (2006).
 - [7] O. V. Skryabina, S. V. Egorov, A. S. Goncharova, A. A. Klimenko, S. N. Kozlov, V. V. Ryazanov, S. V. Bakurskiy, M. Y. Kupriyanov, A. A. Golubov, K. S. Napolskii, and V. S. Stolyarov, *Applied Physics Letters* **110**, 222605 (2017).
 - [8] S. Goswami, E. Mulazimoglu, A. M. R. V. L. Monteiro, R. Wölbing, D. Koelle, R. Kleiner, Y. M. Blanter, L. M. K. Vander-sypen, and A. D. Caviglia, *Nature Nanotechnology* **11**, 861 (2016).
 - [9] E. E. Mitchell and C. P. Foley, *Superconductor Science and Technology* **23**, 065007 (2010).
 - [10] Y. Y. Divin, U. Poppe, C. L. Jia, P. M. Shadrin, and K. Urban, *Physica C: Superconductivity* **372-376**, 115 (2002).
 - [11] N. Bergeal, X. Grison, J. Lesueur, G. Faini, M. Aprili, and J. P. Contour, *Applied Physics Letters* **87**, 102502 (2005).
 - [12] N. Bergeal, J. Lesueur, M. Sirena, G. Faini, M. Aprili, J. P. Contour, and B. Leridon, *Journal Of Applied Physics* **102**, 083903 (2007).
 - [13] M. Malnou, C. Feuillet-Palma, C. Ulysse, G. Faini, P. Febvre, M. Sirena, L. Olanier, J. Lesueur, and N. Bergeal, *Journal Of Applied Physics* **116**, 074505 (2014).
 - [14] S. Ouanani, J. Kermorvant, C. Ulysse, M. Malnou, Y. Lemaître, B. Marcilhac, C. Feuillet-Palma, N. Bergeal, D. Crété, and J. Lesueur, *Superconductor Science and Technology* **29**, 094002 (2016).
 - [15] E. R. Pawlowski, J. Kermorvant, D. Crété, Y. Lemaître, B. Marcilhac, C. Ulysse, F. Couedo, C. Feuillet-Palma, N. Bergeal, and J. Lesueur, *Superconductor Science and Technology* **31**, 095005 (2018).
 - [16] F. Couedo, E. Recoba Pawlowski, J. Kermorvant, J. Trastoy, D. Crété, Y. Lemaître, B. Marcilhac, C. Ulysse, C. Feuillet-Palma, N. Bergeal, and J. Lesueur, *Applied Physics Letters* **114**, 192602 (2019).
 - [17] S. A. Cybart, E. Y. Cho, T. J. Wong, B. H. Wehlin, M. K. Ma, C. Huynh, and R. C. Dynes, *Nature Nanotechnology* **10**, 598 (2015).
 - [18] E. Y. Cho, M. K. Ma, C. Huynh, K. Pratt, D. N. Paulson, V. N. Glyantsev, R. C. Dynes, and S. A. Cybart, *Applied Physics Letters* **106**, 252601 (2015).
 - [19] A. Gozar, N. E. Litombe, J. E. Hoffman, and I. Bozovic, *Nano Letters* **17**, 1582 (2017).
 - [20] E. Y. Cho, H. Li, J. C. LeFebvre, Y. W. Zhou, R. C. Dynes, and S. A. Cybart, *Applied Physics Letters* **113**, 162602 (2018).
 - [21] E. Y. Cho, Y. W. Zhou, J. Y. Cho, and S. A. Cybart, *Applied Physics Letters* **113**, 022604 (2018).
 - [22] B. Müller, M. Karrer, F. Limberger, M. Becker, B. Schröppel, C. J. Burkhardt, R. Kleiner, E. Goldobin, and D. Koelle, *Physical Review Applied* **11**, 044082 (2019).
 - [23] L. Kasaei, T. Melbourne, V. Manichev, L. C. Feldman, T. Gustafsson, K. Chen, X. X. Xi, and B. A. Davidson, *AIP Advances* **8**, 075020 (2018).
 - [24] L. Kasaei, V. Manichev, M. Li, L. C. Feldman, T. Gustafsson, Y. Collantes, E. Hellstrom, M. Demir, N. Acharya, P. Bhattacharai, K. Chen, X. X. Xi, and B. A. Davidson, *Superconductor Science and Technology* **32**, 095009 (2019).
 - [25] H. J. Kwon, K. Sengupta, and V. M. Yakovenko, *The European Physical Journal B* **37**, 349 (2004).
 - [26] R. Gross, P. Chaudhari, M. Kawasaki, and A. Gupta, *Physical review B* **42**, 10735 (1990).
 - [27] A. Marx and R. Gross, *Applied Physics Letters* **70**, 120 (1997).

- [28] D. Gustafsson, F. Lombardi, and T. Bauch, *Physical review B* **84**, 184526 (2011).
- [29] K. Likharev, *Dynamics of Josephson junctions and circuits-Gordon and Breach Science Publishers (1986)*, edited by G. a. Breach (1986).
- [30] Ceraco gmbh.
- [31] P. G. De Gennes, *Review of Modern Physics* **36**, 225 (1964).
- [32] F. Kahlmann, A. Engelhardt, J. Schubert, W. Zander, C. Buchal, and J. Hollkott, *Applied Physics Letters* **73**, 2354 (1998).
- [33] K. Likharev and V. K. Semenov, **15**, 442 (1972).
- [34] Y. Divin, O. Polyanskii, and A. Shul'Man, *Pisma Zh. Tekh. Fiz.* **6**, 1056 (1980).
- [35] Y. Y. Divin and N. A. Mordovets, *Sov. Tech. Phys. Lett.* **9**, 108 (1983).
- [36] Y. Y. Divin, J. Mygind, N. F. Pedersen, and P. Chaudhari, *Applied Physics Letters* **61**, 3053 (1992).
- [37] A. Sharafiev, M. Malnou, C. Feuillet-Palma, C. Ulysse, P. Febvre, J. Lesueur, and N. Bergeal, *Superconductor Science and Technology* **29**, 1 (2016).
- [38] A. J. Dahm, A. Denenstien, D. N. Langenberg, W. H. Parker, D. Rogovin, and D. J. Scalapino, *Physical Review Letters* **22**, 1416 (1969).
- [39] M. Kawasaki, P. Chaudhari, and A. Gupta, *Physical Review Letters* **68**, 1065 (1992).
- [40] M. Liatti, U. Poppe, and Y. Divin, **88**, 152504 (2006).
- [41] A. H. Miklich, J. Clarke, M. S. Coleclough, and K. Char, *Applied Physics Letters* **60**, 1899 (1992).
- [42] Y. Y. Divin, J. Mygind, N. F. Pedersen, and P. Chaudhari, *Applied Superconductivity, IEEE Transactions on* **3**, 2337 (1993).
- [43] L. Hao, J. C. Macfarlane, and C. M. Pegrum, *Superconductor Science and Technology* **9**, 678 (1996).
- [44] A. Marx, U. Fath, W. Ludwig, R. Gross, and T. Amrein, *Physical review B* **51**, 6735 (1995).
- [45] L. Hao and J. C. Macfarlane, *Physica C-Superconductivity And Its Applications* **292**, 315 (1997).
- [46] A. T. Cortez, E. Y. Cho, H. Li, D. Cunnane, B. S. Karasik, and S. A. Cybart, *Ieee Transactions On Applied Superconductivity* **PP**, 1 (2019).